Reinforcement of Si_3N_4 Nanoparticles in Polypropylene Single Fibers Through Melt Extrusion Process and Their Properties

Vijaya K. Rangari, Yousuf M. Shaik, Ghouse M. Mohammad, Shaik Jeelani

Materials Science and Engineering, Center for Advanced materials, Tuskegee University, Tuskegee, Alaska 3608

Received 20 April 2010; accepted 30 October 2010
DOI 10.1002/app.33683
Published online 3 March 2011 in Wiley Online Library (wileyonlinelibrary.com).

ABSTRACT: We have successfully aligned/dispersed the rod and spherical-shaped Si_3N_4 nanoparticles in the polypropylene (PP) fibers through melt extrusion process to fabricate polymer nanocomposite (PNC) single fibers. The alignment/dispersion of Si_3N_4 nanoparticles in PP/Si_3N_4 PNC fibers has been carried out in a systematic manner to produce uniform single fibers. The PNC fibers were first uniformly stretched and stabilized using a two-set Godet machine. The as-extruded single PNC fibers were tested for their thermal and tensile properties. The test results of PNC fibers were compared to neat PP polymer single fibers fabricated using the same procedure as PNC fibers. These results show that the PNC fibers are much (307%) higher in tensile strength and modulus (>1000%) when compared with the neat PP polymer single fibers. The field emission scanning electron microscope results clearly show the alignment of rod-Si_3N_4 nanoparticles in polymer matrix. The differential scanning calorimetry results show $\sim$ 12% increase in crystallinity for rod-Si_3N_4 PNCs when compared with the neat PP single fibers. © 2011 Wiley Periodicals, Inc. J Appl Polym Sci 121: 1512–1520, 2011

Key words: nanocomposites; fibers; reinforcements; extrusion; thermal properties

INTRODUCTION

Polymer nanocomposites (PNCs) have garnered great academic and industrial interest since their inception.[1] PNCs have been shown to enhance physical, thermomechanical, and processing characteristics compared to their neat polymer counterparts. These PNCs can be tailored according to the applications and requirements by the selection of nanoparticles morphology and compatible polymer matrices. Polymers such as PP-6, polypropylene (PP), and LDPE when mixed with appropriate percentage of nanoparticles as fillers show significant improvements[2–4] in their mechanical and thermal properties. Among the thermoplastics, PP is one of the most commonly used polymers, and their potential applications as cost-effective replacements of engineering polymers have attracted considerable attention and have been widely investigated.[5,6] However, PP is brittle under severe conditions of deformation, such as at low temperatures or high impact rates, which has limited its wider range of engineering applications. Incorporation of rigid inorganic particles is a promising approach to improve both stiffness and toughness of plastics simultaneously.[7–10] Recent literature survey clearly shows that most of the work on PP-PNCs was carried out using CNTs,[11,12] CNFs,[13] $CaCO_3$,[14,15] hydroxyapatite,[16] calcium phosphate,[17] POSS,[3] and clay particles as fillers. Comparatively, PP/clay nanocomposites have been extensively studied.[18,19] Mostly, the purpose of these studies is to reduce the cost, improve the mechanical, and fire-retardency properties. PP fibers have been widely used in apparel, upholstery, floor coverings, hygiene medical, geotextiles, car industry, automotive textiles, various home textiles, and wall coverings.[20] As far as we know, there was no published report on the PNCs of PP fibers containing nano-Si_3N_4 particles.

Nanostructured silicon nitride particles exhibit a high potential for the reinforcement of polymers.[21–24] Silicon nitride is considered to be a promising ceramic because of its exceptional chemical and mechanical properties, especially at high temperature.[25] In this present study, we have chosen rod and spherical Si_3N_4 nanoparticles as fillers and PP as polymer matrix to produce high-strength PNCs.

A significant progress has been made in dispersion of acicular or spherical nanoparticles in polymer matrix by surface modification and other techniques. Whereas alignment of acicular or rod-shaped particles in polymeric fiber and manufacturing advanced macrosopic structures remains a challenge. Most commonly,

Correspondence to: V. K. Rangari (rangariv@tuskegee.edu).

Contract grant sponsor: National Science Foundation (through NSF-PREM, RISE and Alabma EPSCoR grants).

using techniques for alignment are wet spinning,[26] magnetic alignment[27] electrospinning,[28] and melt processing.[29,30] To align the nanoparticles while extruding, many aspects should be considered such as the starting materials and their chemical compositions, their mixing techniques. The type of extruder, material-loading process, extrusion temperature, material residence time within the extruder, the die and its orifice shape and size, extrusion rate, extrusion direction, surrounding air temperature and its speed, fibers cooling type and process, filament draw ratio, and winding speed are also very important. Proper combination of such factors leads to the production of fine fibers.

In the recent years, much attention has been paid to the synthesis of different morphologies of silicon nitride nanoparticles compounds. The spherical and rod-shaped morphologies are studied extensively among them. Our present interest deals with the study of both of these morphologies of silicon nitride nanoparticles along with PP. Both neat and nanoparticle-infused PP single fibers were produced using a single screw extrusion technique. Morphological, thermal, and mechanical properties are presented in this work.

EXPERIMENTAL

Materials

The Si_3N_4 nanorods (light gray color, Si_3N_4 alpha, 99%, and size 100 $\times$ 800 nm) and spherical-shaped (white color, Si_3N_4 amorphous, 98.5+%, and size 15–30 nm) particles were obtained from *Nanostructured and Amorphous Materials* and TEM picture as shown in Figure 5(c,d), respectively. PP (Microthene FP-800-00 micro-fine powder $\sim$ 20 μm, melt flow rate 35 g/10 min, and density $\sim$ 0.909 g/cc) powder was purchased from Equistart Chemicals, LP, and scanning electron microscopy (SEM) picture is shown in Figure 5(a).

Melt processing

Rod-shaped Si_3N_4 particles and PP powder were carefully measured in the ratio of 1 : 99 by weight (1 wt %) and dry mixed using a mechanical blender at a speed of 2300 rpm with a circulating cold base container (5°C). The mixing process was paused for 6 min after 3 min of continuous mixing and then resumed for further mixing. This was done to avoid temperature rise, which may result in softening the PP. This technique is repeated 20–30 times until uniform mixing was observed. The effective time for which the mixture was blended was between 75 and 90 min. At this time, the mixture took a light gray appearance, and it seemed that the rod Si_3N_4 particles were thoroughly mixed with the PP. The same process was repeated for the spherical Si_3N_4 nanoparticle mixing with PP polymer to ensure proper blending.

The mixture of PP and Si_3N_4 nanoparticles was then further air dried in a dryer for 12 h and extruded using a *Wayne Yellow Label Table Top single screw extruder* (Fig. 1). Thermostatically controlled five heating zones were used to melt the mixture before extrusion; three of which were occupied by the barrel zone and rest of the two were by the die zone. The heaters inside the barrel zone were placed at the feed hopper side, center and die zone side of the barrel, and set at a temperature of 167.5, 171.5, and 173.5°C, respectively. The process begins when the nanophased dry-mixed powder is poured through the feed hopper to get inside the barrel zone of the extruder. As soon as they reach the barrel zone, PP starts melting due to high barrel temperature. At this stage, the whisker particles are randomly distributed within the liquid matrix. The outer surface of the screw is designed to maintain close fit with the barrel inner surface and molten mass trapped inside the screw segment. As the extruder screw rotates, this molten matrix partially mixed with the nanoparticles, conveyed in a spiral pattern and finally reaches the screw end, which is located immediately before the die zone. The screw end is shaped in such a way that it allows the flowing mass to escape through a narrow openings at high velocity. As the screw rotation is continued, the high velocity liquid experiences enormous shear force. The shear force at this high temperature can alter the chemical and thermal properties of the PP and the orientation of rod-shaped particles. It is assumed that the rod-shaped particles are partially aligned at this stage. The partially aligned rod-shaped particles containing liquid PP now enters the die zone. It should be noted that to ensure proper alignment of fiber, the size of the die plate and the diameter of the die opening are very critical. Hence, a specially designed die was used in this process, which has a converging inlet and narrow outlet (1 mm). This die configuration generates two distinct flow regimes that highly affect the fiber alignments. First, the converging die inlet introduces a converging flow pattern, which, in turn, aligns the fibers along the streamline direction. Second, the narrow orifice allows the flow pattern to transform into shear flow as it enters the narrow orifice. The shear flow produces additional fiber alignment due to differential shear rate along the boundary layer that orients the fibers in the direction of flow.[26,27]

This process is continuous, and the composite fibers with constant tension were extruded at a screw speed of 8–10 rpm and feed rate of $\sim$ 100 g/h. These fibers were allowed to travel from the water bath (20°C) to a set of tension rollers, winder guide rollers, and then wound on a spool (*Wayne Desktop Filament Winder*) at

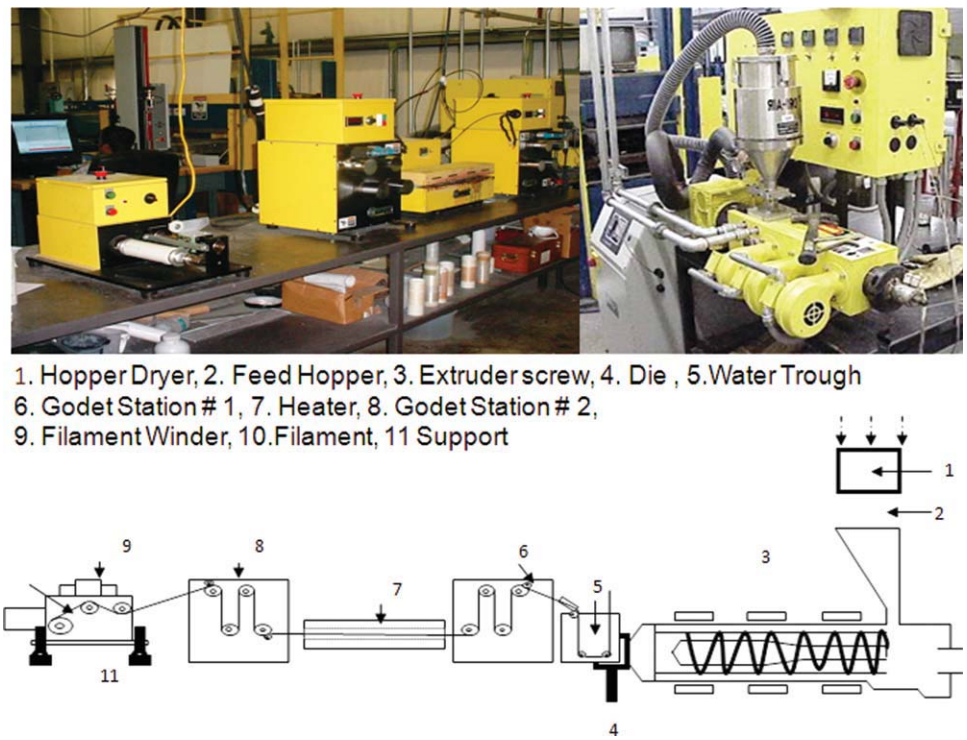

Figure 1 Single screw polymer fiber extrusion setup. [Color figure can be viewed in the online issue, which is available at wileyonlinelibrary.com.]

a winding speed of 45 rpm. The process temperature, speed ratio between the winder and extruder screw, position of the roller guide, and filament travel distance, all these factors control the draw ratio λ (ratio of die orifice diameter to filament final diameter) of the process as well as the continuity of the fibers.

Testing procedures

Differential scanning calorimetry (DSC) experiments were carried out using a Mettler Toledo DSC 822^e from 30 to 300°C at a heating rate of 5°C/min under nitrogen atmosphere and cooled from 300 to 30°C at the same heating rate and atmosphere. The degree of crystallinity was determined from the melting endotherm. The percentage of crystallinity was calculated using the following Eq. (1):

$$H^*(\%) = \frac{\Delta H_m \Big/ \phi_{pp}}{\Delta H_m^o} \times 100$$

where ΔH_m is the melting enthalpy calculated from the area under the curve of melting endotherm, ϕ_{pp} is the weight fraction of PP in the nanocomposite, and ΔH_m^o is enthalpy of fusion of 100% crystalline PP ($\Delta H_m^o = 209$ J/g).[31,32]

The as-received polymer powder, rod-Si_3N_4, spherical-Si_3N_4 particles, and their PNC fibers were analyzed for their shape and sizes using JEOL-2010 transmission electron microscopy (TEM) and JEOL-5800 SEM. For TEM analysis, the sample grids were prepared by dropping a drop of colloidal solution of powdered sample in ethanol on a conversional carbon-coated copper (200-mesh) grid. To study the alignment/dispersion of Si_3N_4 in PP polymer, fibers were examined using *JEOL FE-JSM7000F* field emission scanning electron microscope (FE–SEM). The as-prepared PP fibers were placed on a double-sided carbon tape and coated with gold palladium to avoid the sample charging. To corroborate the alignment of the rod-Si_3N_4 in the PP polymer matrix, the polymer was etched and coated with gold palladium before the FE–SEM analysis. Etching of the specimens was carried out in a HUMMER 6.2 Sputtering system with aluminum target. The etching process was done in the argon atmosphere for a span of 1 h. The vacuum was maintained between 60 and 80 mtorr, and the current flow was maintained between 10 and 15 Å. Because of etching, most of the polymer that covered the matrix layer facing the target was etched out, and the Si_3N_4 nanorods were clearly seen in the FE–SEM. Tensile tests were conducted on a Zwick/Roell tensile tester with 20-N load cell. Test specimens were cut and each of fibers were aligned to the two ceramic grips, with a distance of separation of 102 mm (gauge length). A minimum of 10 tensile tests were conducted to obtain the consistence average values.

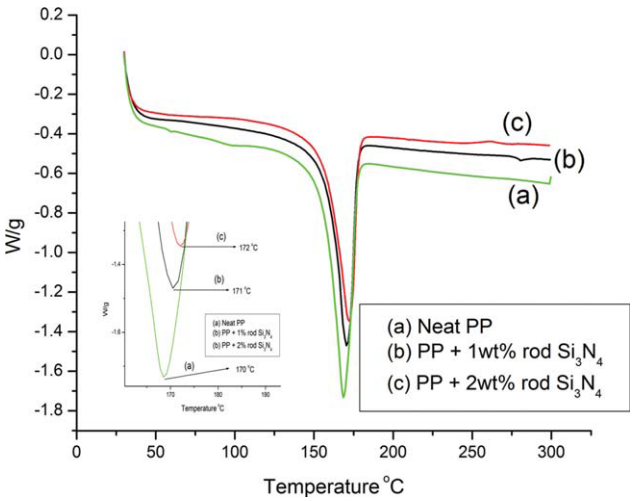

Figure 2 The DSC melting curves of (a) neat PP, (b) 1 wt % rod-Si3N4/PP, and (c) 2 wt % rod-Si3N4/PP. Inset figure shows the melting points at closer look. [Color figure can be viewed in the online issue, which is available at wileyonlinelibrary.com.]

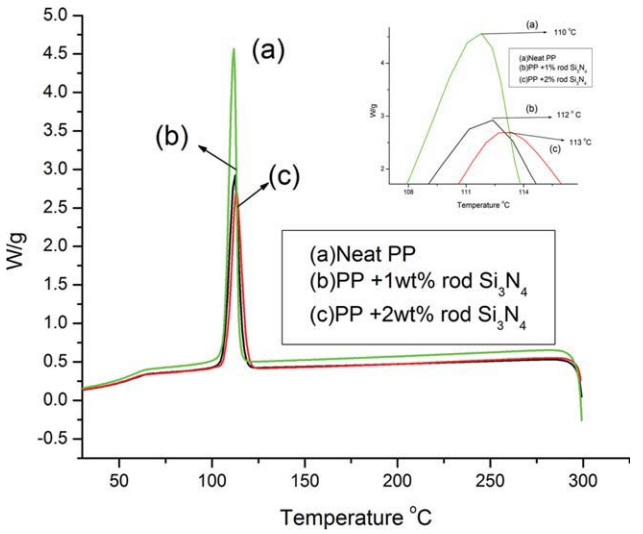

Figure 3 The DSC cooling curves of (a) neat PP, (b) 1 wt % rod-Si3N4/PP, and (c) 2 wt % rod-Si3N4/PP. Inset figure shows the crystallization points at a closer look. [Color figure can be viewed in the online issue, which is available at wileyonlinelibrary.com.]

RESULTS AND DISCUSSION

The effect of rod-Si_3N_4 and sph-Si_3N_4 on melting and crystallization temperature of PP was studied by measuring the heating and cooling response using DSC. Figure 2 depicts the melting curves of (a) neat PP, (b) 1 wt % rod-Si_3N_4/PP, and (c) 2 wt % rod-Si_3N_4/PP, and the results are summarized in Table I. The melting enthalpy calculated from melting curves indicates that the enthalpy values increased for 1 wt % rod-Si_3N_4/PP (81.14 J/g) and 2 wt % rod-Si_3N_4/PP (100.21 J/g) when compared with neat PP (78.62 J/g). These results clearly suggest that the melting enthalpy affected significantly by the addition of rod-Si_3N_4 nanoparticles. The crystallinity of the polymer calculated using the Eq. (1) shows that the crystallinity is increased by the addition of 1 wt % rod-Si_3N_4/PP (39.2%) and 2 wt % rod-Si_3N_4/PP (48.9%), respectively, when compared with neat PP (37.3%). In the cooling curve, as expected, the recrystallization temperature (shown in Fig. 3) is also increased from 110°C (neat PP) to 113°C (2 wt % rod Si_3N_4). The reason for the increase in crystallinity of PP may be Si_3N_4 nanoparticles acting as nucleating agents to initiate the initial crystallization of PP. These results further confirm the increase in crystallinity of rod-Si_3N_4 infused PP. These results are also consistent with other reports on similar systems such as infusion of $CaCO_3$ nanoparticles in PP.[33] It is also reported that the higher (10–25 wt %) percentages of larger particle (25 μm) sizes loading in PP show the decrease in crystallinity.[34] This decrease in crystallinity is in contradiction to the common belief that the introduction of nanoparticles into the polymer melt would enhance the nucleation of crystallites in the polymer. It is also well known that increase in crystallinity increases the mechanical properties.[29,30,35,36] To further understand the effect of reinforcement, we have also studied the crystallinity of sph-Si_3N_4 nanoparticle-infused PP. These spherical Si_3N_4 nanoparticles are much smaller and amorphous in nature. Figure 4 shows the DSC melting curve of 1 and 2 wt % of sph-Si_3N_4 nanoparticle-infused PP. The melting enthalpy measured for 1 wt % sph-Si_3N_4 infused in PP is ~ 97.05 J/g and 84.20 for 2 wt % sph-Si_3N_4 infused in PP. These melting enthalpies are much higher when compared with

TABLE I
DSC Results of Neat PP, Rod-Si_3N_4/PP, and sph-Si_3N_4/PP Fibers

Sample	Melting temperature (°C)	Melting enthalpy (J/gm)	Recrystalization temperature (°C)	% Crystallinity
Neat PP	170	78.62	110	37.3
PP + 1 wt % rod-Si_3N_4	171	81.14	112	39.2
PP + 2 wt % rod-Si_3N_4	172	100.21	113	48.9
PP + 1 wt % sph-Si_3N_4	170	97.05	113	46.9
PP + 2 wt % sph-Si_3N_4	172	84.20	115	41.1

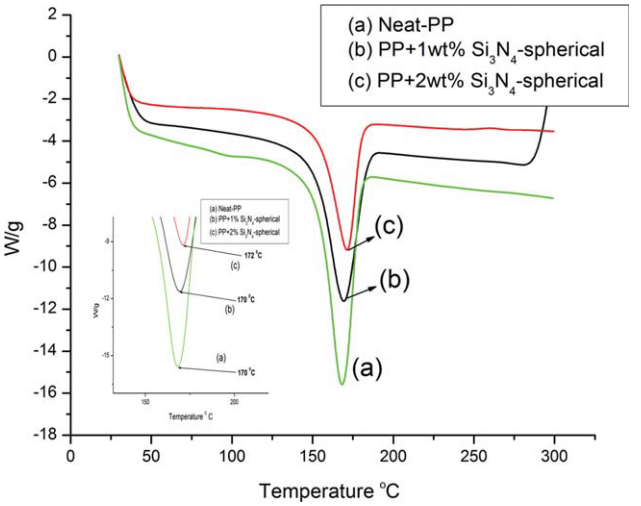

Figure 4 The DSC melting curves of (a) neat PP, (b) 1 wt % sph-Si3N4/PP, and (c) 2 wt % sph-Si3N4/PP. Inset figure shows the melting points at closer look. [Color figure can be viewed in the online issue, which is available at wileyonlinelibrary.com.]

the neat PP (78.62 J/g) melting enthalpy. These results also clearly suggest that the melting enthalpy affected significantly by the addition of spherical-Si_3N_4 nanoparticles as well. The crystallinity calculated using the Eq. (1) show that the crystallinity is increased by the addition of 1 wt % sph-Si_3N_4/PP (46.9%) and 2 wt % sph-Si_3N_4/PP (41.1%), respectively, when compared with neat PP (37.3%). In the cooling curve, as expected, the recrystallization temperature as shown in Figure 5 is also increased from 110°C (neat PP) to 115°C (2 wt % spherical Si_3N_4). As explained earlier, the reason for increase in crystallinity of PP is also may be Si_3N_4 particles acting as nucleating agents to initiate initial crystallization of PP. These results further confirm the increase in crystallinity of sph-Si_3N_4-infused PP, and these results are consistent with rod-Si_3N_4 nanoparticles. As expected, the crystallinity of 2 wt % spherical Si_3N_4-infused PP increased almost 2% more than that of 2 wt % rod Si_3N_4 nanoparticles infused in PP. The reason for increase in crystallinity of PP may be spherical Si_3N_4 nanoparticles activity of acting as nucleating agents to initiate initial crystallization of PP is more than that in the case of rod-Si_3N_4 nanoparticles because of their smaller size, high reactivity, and amorphous nature.

Morphological studies

The SEM images in Figure 6(d–f) show the surfaces and diameters of continues single fibers of (d) neat PP, (e) 1 wt % sph-Si_3N_4/PP, and (f) 1 wt % rod-Si_3N_4/PP.

The surfaces of these fibers are almost smooth and uniform, and no defects were observed along the length of the fiber. The diameters measured for these single fibers are ~ 130, 110, and 150 μm, respectively, for (d) neat PP, (e) 1 wt % sph-Si_3N_4/PP, and (f) 1 wt % rod-Si_3N_4/PP. These diameters were used to calculate the tensile strength of single fibers. FE–SEM (*JEOL FE-JSM7000F*) studies have been carried out to study the alignment of rod-Si_3N_4 in PP fibers. To corroborate the alignment of the Si_3N_4 rods in PP matrix, the polymer was initially etched and coated with gold palladium before the FE–SEM analysis. Etching of the specimens was carried out in a HUMMER 6.2 plasma-etching system with aluminum target. The etching process was done in the argon atmosphere for a span of 1 h. The vacuum was maintained between 60 and 80 mtorr, and the current flow was maintained between 10 and 15 Å. The samples for FE–SEM experiments were prepared by plasma etching the as-extruded rod-Si_3N_4/PP fibers in argon gas for 30 min. Because of the etching, most of the polymer that covered the matrix layer facing the target was etched out, and the Si_3N_4 rods were clearly seen in the FE–SEM. Figure 7(a) clearly shows that the rod-shaped Si_3N_4 particles are aligned in the fiber extrusion direction. These Si_3N_4 particles were surfaced only after deep etching of the surface polymer. Such alignment of the rod-shaped particles proves the ability of the extrusion method to align the particles in the fiber extrusion direction. To find out the alignment of rod-Si_3N_4 particles deep in the fiber, a higher magnification FE–SEM was carried out and depicted in Figure 7(b). This micrograph shows a single rod-shaped Si_3N_4 particle straight along the fiber extrusion direction. Figure 7(c,d) shows the FE–SEM micrograph of tensile fracture surfaces of rod-Si_3N_4 fiber.

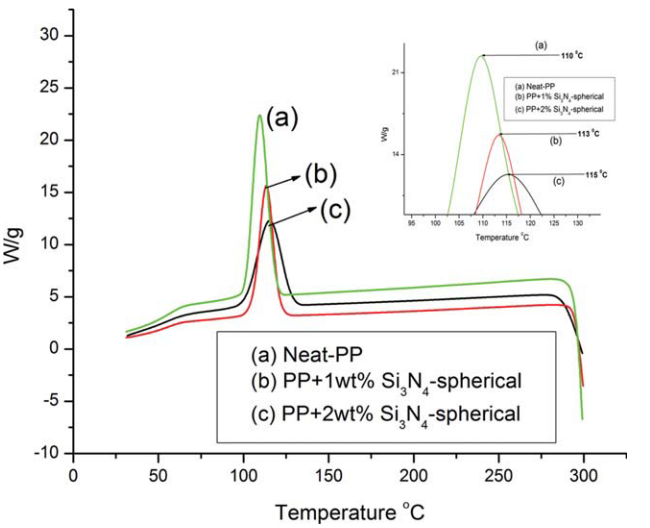

Figure 5 The DSC cooling curves of (a) neat PP, (b) 1 wt % sph-Si3N4/PP, and (c) 2 wt % sph-Si3N4/PP. Inset figure shows the crystallization points at a closer look. [Color figure can be viewed in the online issue, which is available at wileyonlinelibrary.com.]

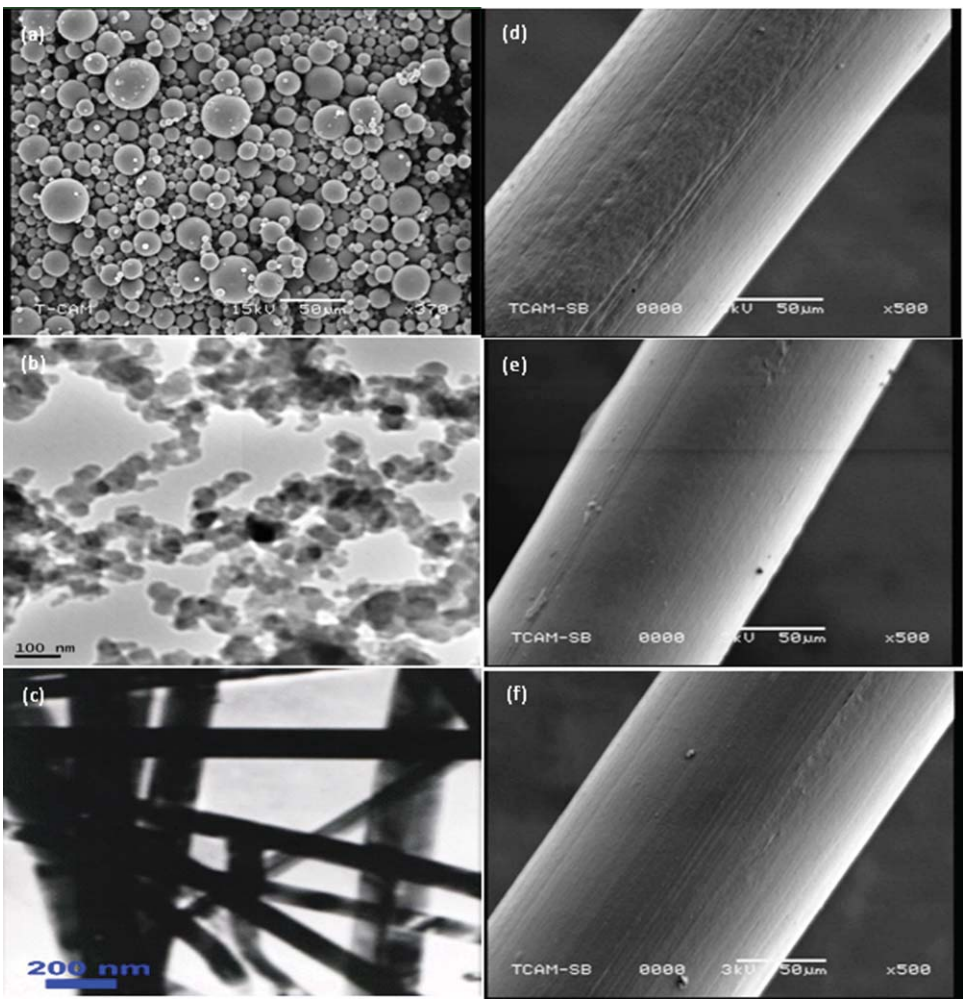

Figure 6 SEM micrograph of (a) as-received PP, (b) TEM micrograph of as-received sph-Si3N4, (c) as-received rod-Si3N4 and SEM micrographs of (d) neat PP, (e) 1 wt % sph-Si3N4/PP, and (f) 1 wt % rod-Si3N4/PP fibers. [Color figure can be viewed in the online issue, which is available at wileyonlinelibrary.com.]

These micrographs clearly show that the PP polymer chains are entangled and exfoliated on the rod-Si_3N_4 particles. Figure 7(d) also sees the particles pullout from the polymer matrix and uniform dispersion of rod-Si_3N_4 nanoparticles in polymer matrix. The rod-Si_3N_4 nanoparticles are aligned/dispersed in PP fiber in different layers one below the other layers. The micrograph clearly shows that the rod-shaped particles are in the various levels of the fiber thickness. This phenomenon plays the leading role in enhancing the mechanical properties of composite fibers.

Tensile response

Tensile tests were carried out to study the effect of alignment of rod-Si_3N_4 particles in PP polymer on tensile strength and modulus. The single fiber tests were carried out according to the ASTM standard D 3379-75[37] using Zwick/Roell tensile testing equipment with a 20-N load cell. Test specimens were cut and each of these fibers were aligned to the two ceramic grips, with a distance of separation of 102 mm (gauge length). The fiber dimensions were measured using SEM for accuracy. The tensile stress–strain curve is shown in Figure 8, and the data are summarized in Table II. The ultimate tensile strength of 1 and 2 wt % of rod-Si_3N_4/ PP is 249.48 and 307.21 MPa, respectively, whereas the neat PP is 63.58 MPa. These results show that the ultimate tensile strength is increased by 383% when compared with that of neat PP. To understand further the effect of reinforcement, we have also studied the tensile properties of sph-Si_3N_4 nanoparticles infused in PP, and the results are summarized in Table II and shown in Figure 9. The ultimate tensile strength of 1 and 2 wt % of sph-Si_3N_4/ PP is 193.07 and 236.76 MPa, respectively. These results clearly shows that the reinforcement of rod-Si_3N_4 nananoparticles in PP is higher (70.48 MPa) in strength when compared with the sph-Si_3N_4 nanoparticle in PP. The

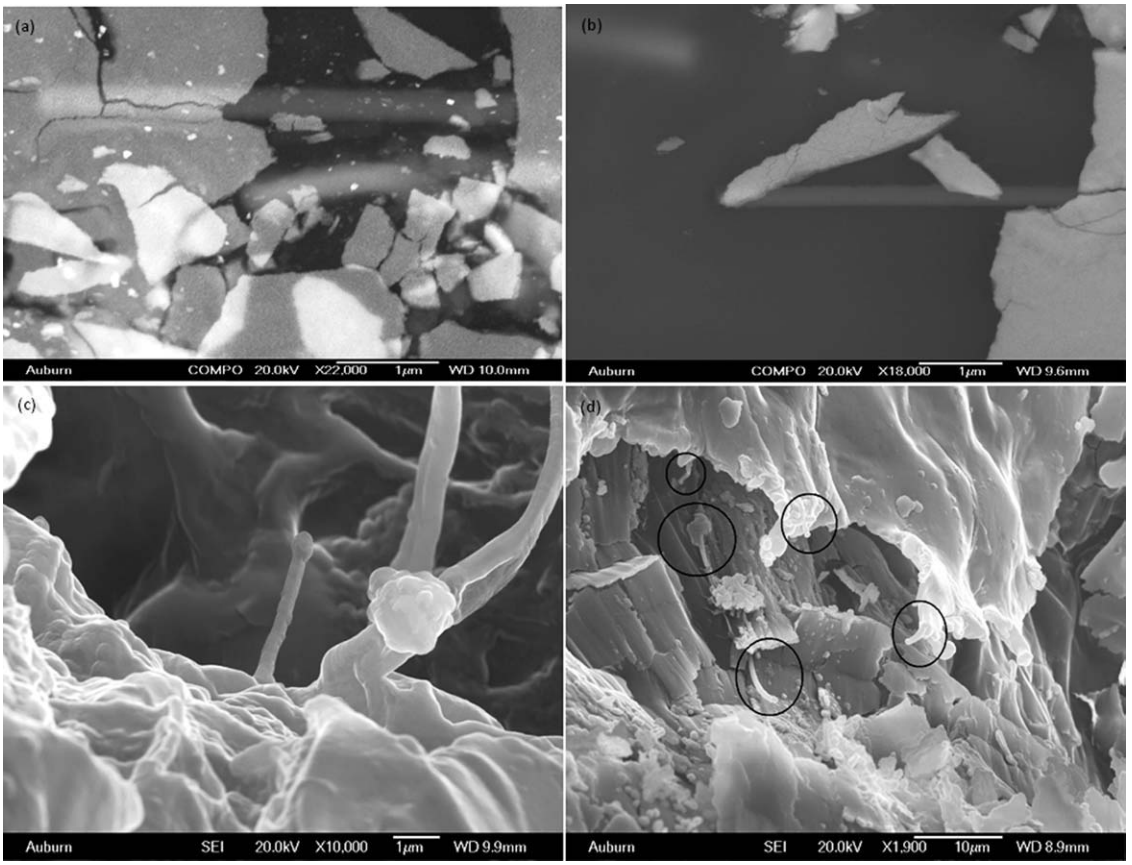

Figure 7 FE–SEM micrographs of (a) and (b) aligned rod-Si3N4 in PP matrix and (c) and (d) rod-Si3N4/PP tensile fracture surface.

main reason for this may the alignment of rod-Si_3N_4 nanoparticles in fiber extrusion direction (tensile), which may not be significant in the case of sph-Si_3N_4 nanoparticles alignment in PP fibers. The tensile modulus was calculated from the stress versus strain curve (Figs. 8 and 9) of neat PP, and 1 and 2 wt % of rod-Si_3N_4 and sph-Si_3N_4 are 0.49, 4.03, 5.03, 4.05, and 4.37 GPa, respectively. This strength/modulus of 2 wt % rod-Si_3N_4 nanocomposite fiber 307 MPa/5.03.4 GPa) is more than that of the neat PP (63.58 MPa/0.49 GPa), which indicates the exceptional load-bearing capability of rod-Si_3N_4 and their potential applications in structural composite materials.

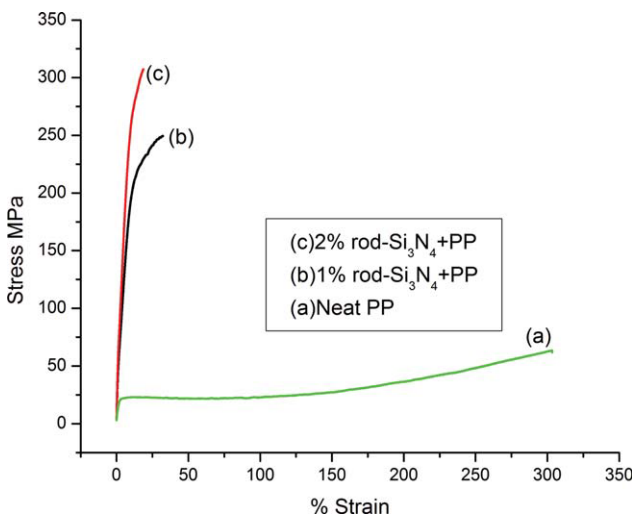

Figure 8 Tensile response of (a) neat PP, (b) 1 wt % rod-Si3N4/PP, and (c) 2 wt % rod-Si3N4/PP. [Color figure can be viewed in the online issue, which is available at wileyonlinelibrary.com.]

The reason for high increments in tensile properties is may be due to the alignment and exfoliation of rod-shaped Si_3N_4 particles in PP polymer. These significant improvements of tensile modulus were attributed to the infusion of high-strength Si_3N4 nanoparticles

TABLE II
Tensile Response of Neat PP, Rod-Si_3N_4/PP, and sph-Si_3N_4/PP Fibers

Type	Tensile strength (MPa)	% Improvement	Tensile modulus (GPa)
Neat PP	63.58	–	0.49
PP + 1 wt % rod-Si_3N_4	249.48	292	4.03
PP + 2 wt % rod-Si_3N_4	307.21	383	5.03
PP + 1 wt % sph-Si_3N_4	193.07	204	4.05
PP + 2 wt % sph-Si_3N_4	236.76	272	4.37

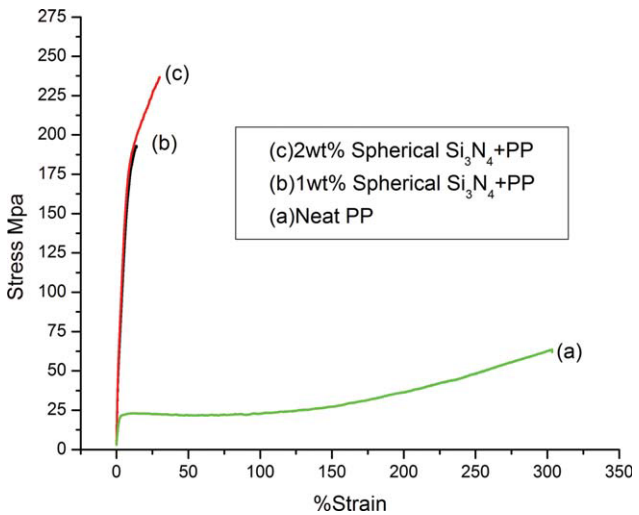

Figure 9 Tensile response of (a) neat PP, (b) 1 wt % sph-Si3N4/PP, and (c) 2 wt % sph-Si3N4/PP. [Color figure can be viewed in the online issue, which is available at wileyonlinelibrary.com.]

and their alignment in extrusion direction of PP polymer filaments. These results are consistent with the FE–SEM analysis and also with our previous results (179% for strength and 276% for modulus practically without any loss of fracture strain)[29] on Si_3N_4 rod-shaped and spherical nanoparticles infused in Nylon-6. As we discussed earlier in our DSC results, Hao and et al.[38] also reported the crystallization kinetics of PP infuse Si_3N_4 nanocomposites and found that the crystallization temperature of PP nanocomposites with 2 wt % of Si_3N_4 is highest, indicating that the crystallization rate is highest at this loading percentage because of the high nucleation activity of Si_3N_4 at 2 wt % loading. In our case, we also found that the highest crystallization loading is $\sim$ 2 wt % of Si_3N_4 both spherical and rod-shaped particles. In the case of rod-shaped particles, the increase in tensile strength is higher than the spherical particles at the same nanoparticles loading. This suggests that in case of rod-Si_3N_4 particles infusion in PP, the added advantage is the alignment of particles in the extrusion direction. The effects of alignment on tensile properties were observed in our earlier studies as well.[29,30,36,39,40] Recently, Xu and his coworkers[41] also reported their research results on nanoamorphous Si_3N_4 particles in PP polymer. In contrary to our results, they found that the infusion of amorphous Si_3N_4 nanoparticles in PP and the tensile properties nanocomposites were marginally decreased. The reason for this difference may be the variation in the processing technique sample dimensions. In our case, the test samples are in the form of fibers, and particles are rod shaped where the effect of alignment is significant.

In the present study, we have achieved significant improvements in tensile strength and modulus with loss of toughness. Because toughness depends on several factors, it is difficult to increase the toughness by reinforcement of nanoparticles in polymers.[42] Usually, the toughness has been characterized by Izod or Charpy impact energy, which is plastic, work dominating. In the current study, the sample sizes are not suitable for direct impact tests. In general, the toughness decreases with decreasing particle size or amount. In the present study, the toughness of nanocomposites is also decreased drastically when compared with the neat PP. These results are consistent with the other reports in the literature.[13,34] It is well known in the literature that with the addition of most of the nanoparticles to the polymer, they become more brittle and decrease the ductility and toughness of the polymer. We have also repeatedly observed in our earlier studies on infusion of CNTs and nanoparticles coated CNTs in Nylon-6 polymer decrease the toughness.[29,30,36,39] In some cases, the decrease is drastic, and, in others, it is marginal. It depends on the type of nanoparticles and polymer-processing technique. In one of our recent study, we have also observed the increased tensile strength without loss of ductility in case of Nylon-6 infused with SiO_2 nanoparticles.[43] Chan and his coworkers[44] recently reported the marginal to no increase in ductility in case of PP infused with 9.2 wt % $CaCO_3$ nanoparticles at the loss of 12% ultimate tensile strength. To increase the toughness of a thermoplastic polymer, it needs to be modified with plasticizer or infused with a surface modified and hybrid nanoparticles. More studies are needed in this direction to improve the toughness along with strength. The further studies in this direction are in progress.

CONCLUSIONS

We have successfully aligned the rod-Si_3N_4 nanoparticles in PP single fibers through melt extrusion process, and these results are compared to neat PP and sph-Si_3N_4 nanoparticles infused in PP single fibers. The DSC results indicates that the crystallinity is increased $\sim$ 12 and 10% by the addition of 2 wt % rod-Si_3N_4 and 1 wt % sph-Si_3N_4 in PP, respectively, when compared with neat PP. Significant enhancement in tensile properties has been observed for 2 wt % rod-Si_3N_4 nanoparticles infused in PP when compared with the neat PP and sph-Si_3N_4 nanoparticles infused in PP. The tensile results clearly show that these nanocomposite polymer fibers are much (307%) higher in tensile strength and modulus (>1000%) when compared with the neat PP fibers. The FE–SEM results clearly suggest that the rod-Si_3N_4 nanoparticles can be successfully aligned in the fiber direction through melt extrusion process.

References

1. Richard, A. V.; John, F. M. Chem Mater 2007, 19, 2736.
2. Yang, K.; Ozisik, R. Polymer 2006, 47, 2849.
3. Fina, A.; Abbenhuis, H. C. L.; Tabuani, D.; Frache, A. G.; Camino, G.; Polym Degrad Stab 2006, 91, 1064.
4. Kontou, E.; Niaounakis, M. Polymer 2006, 47, 1267.
5. Qian, J.; He, P.; Nie, K. J Appl Polym Sci 2004, 91, 1013.
6. Maiti, P.; Nam, P. H.; Okamoto, M.; Kotaka, T.; Hasegawa, N.; Usuki, A. Polym Eng Sci 2002, 42, 1864.
7. Bartczak, Z.; Argon, A. S.; Cohen, R. E.; Weinberg, M. Polymer 1999, 40, 2347.
8. Thio, Y. S.; Argon, A. S.; Cohen, R. E.; Weinberg, M. Polymer 2002, 43, 3661.
9. Gaymans, W. C. J.; Westzaan, C.; Huetink, J.; Gaymans, R. J. Polymer 2003, 44, 261.
10. Argon, A. S.; Cohen, R. E. Polymer 2003, 44, 6013.
11. William, E.; Dondero, R.; Gorga, E. J Polym Sci Part B: Polym Phys 2006, 44, 864.
12. Masuda, J.; John M. T. Macromolecules 2008, 41, 5974.
13. Peter, H.; Vivien, B.; Ian, W. Polymer 2005, 46, 10936.
14. Ling, Z.; Chunzhong, L.; Rui, H. J Polym Sci Part B: Polym Phys 2004, 42, 1656.
15. Zhanga, Q. X.; Yua, Z. Z.; Xiea, X. L.; Maia, Y. W. Polymer 2004, 45, 5985.
16. Liu, Y.; Wang, M. J Appl Polym Sci 2007, 106, 2780.
17. Saujanya, C.; Radhakrishnan, S. Polymer 2001, 42, 6723.
18. Rácz, L.; Pukánszky, B., Jr.; Pozsgay, A.; Pukánszky, B. Prog Colloid Polym Sci 2004, 125, 96.
19. Hiroaki, M.; Rich, M. J.; Drzal, L. T. Polym Compos 2005, 26, 42.
20. Sheng, Z.; Richard, H. A.; Richard, H.; Baljinder, K. K. Polym Degrad Stab 2006, 91, 719.
21. Zeynep, E.; Miko, C.; Celal, B. Macromol Symp 2002, 185, 259.
22. Weifu, D.; Yiqun, L.; Xiaohong, Z.; Jianming, G.; Fan, H.; Zhihai, S.; Bang, H. T.; Jinliang, Q. Macromolecules 2005, 38, 4551.
23. Zhang, W. D.; Shen, L.; Phang, I. Y.; Tianxi, L. Macromolecules 2004, 37, 256.
24. Liangwei, Q.; Monica, V. L.; Lin, Y.; Kitaygorodskiy, A.; Chen, B.; McCall, A. M.; John, W. C.; Ping, S. Y. Macromolecules 2005, 38, 10328.
25. Lange, F. F. J Am Ceram Soc 1983, 62, 1369.
26. Vigolo, B.; Penicaud, A.; Coulon, C.; Sauder, C.; Pailler, R.; Journet, P. B.; Poulin, P. Science 2000, 290, 1331.
27. Correa-Duarte, M. A.; Grzelczak, M.; Salugueirino-Maceira, V.; Giersig, M.; Liz-Marzán, L. M.; Farle, M.; Sierazdki, K.; Diaz, R. J Phys Chem B 2005, 109, 19060.
28. Ko, F.; Gogotsi, Y.; Ali, A.; Naguib, N.; Ye, H.; Yang, G.; Li, C.; Willis, P. Adv Mater 2003, 15, 1161.
29. Rangari, V. K.; Mohammad, Y. S.; Mahfuz, H.; Jeelani, S. Mater Sci Eng A 2009, 500, 92.
30. Mahfuz, H.; Ashfaq, A.; Mohammad, M. H.; Rangari, V. K.; Jeelani, S.; Steven, D. J. Appl Phys Lett 2006, 88, 83119.
31. Zhang, J. F.; Sun, X. Z. Polym Int 2004, 53, 716.
32. Wunderlich, B. Macromolecular Physics; Academic Press: New York, 1976.
33. Lin, Z.; Huang, Z.; Zhang, Y.; Mai, K.; Zeng, H. J Appl Polym Sci 2004, 91, 2443.
34. Liu, Y.; Wang, M. J Appl Polym Sci 2007, 106, 2780.
35. Fried, J. R. Polymer Science and Technology, 2nd ed.; Prentice Hall: Upper Saddle River, NJ, 2003.
36. Rangari, V. K.; Mohammed, S.; Jeelani, S.; Merlyn X. P.; Valery, N. K. Nanotechnology 2008, 19, 245703.
37. American Society for Testing Materials ASTM Standard D3379–75, "Tensile Strength and Young's Modulus for High-Modulus Single-Filament Materials."
38. Hao, W.; Yang, W.; Cai, H.; Huang, Y. Polym Test, 1020, 29, 527.
39. Rangari, V. K.; Mohammad, G.; Jeelani, S.; Butenko, Y.; Dhanak, V. ACS Appl Mater Interf 2010, 7, 1829.
40. Rangari, V. K.; Mohammad, G.; Jeelani, S.; Angel, H.; Komal, V.; Shree, R. S.; Shreekumar, P. Nanotechnology 2010, 21, 095102.
41. Xu, G. C.; Wang, J.; Ji, X. L.; Xiong, J. Y.; Li, F. J Compos Mater 2007, 41, 2213.
42. Cotterell, B.; Chia, J. Y. H.; Hbaieb, K. Eng Fract Mech 2007, 74, 1054.
43. Mahfuz, H.; Mohammad, M. H.; Rangari, V. K.; Jeelani, S. Macromol Mater Eng 2007, 292, 437.
44. Chan, C. M.; Wu, J.; Li, X. J.; Cheung, K. Y. Polymer 2002, 43, 2981.